ELECTRONIC SUPPLEMENTARY INFORMATION

Cobalt sandwich-stabilized rhodium nanocatalysts for ammonia borane and tetrahydroxydiboron hydrolysis

Qiuxia Zhao,[a,b] Bruno Espuche,[c,d] Naixin Kang,[a] Sergio Moya[c] and Didier Astruc[a,*]

[a] ISM, UMR CNRS N° 5255, Univ. Bordeaux, 33405 Talence Cedex, France.

[b] LCC, CNRS & Univ. Toulouse III, 205 Route de Narbonne, 31077 Toulouse Cedex, France.

[c] Soft Matter Nanotechnology Lab, CIC biomaGUNE, Paseo Miramón 182. 20014. Donostia-San Sebastián, Gipuzkoa, Spain.

[d] POLYMAT, Applied Chemistry Department, Faculty of Chemistry, University of the Basque Country, UPV/EHU, Paseo Manuel de Lardizabal 3, Donostia-San Sebastián, 20018, Spain

Contents

1. General data

All solvents and chemicals were used as purchased. Before usage, all the flasks were washed with a solution of aqua regia (HCl/HNO$_3$ = 3:1 v/v) in order to avoid metal residues. Milli-Q water (18.2 MΩ) was used for all the nanoparticle preparations.

--NMR spectra were recorded at 25 °C with a Bruker AC 300 MHz. All the chemical shifts are reported in parts per million (δ, ppm) with reference to Me4Si for the ^{1}H NMR spectra.

--**Transmission Electron Microscopy (TEM)** were recorded on TEM JEOL JEM 1400 (120 kV) - 2100F.

UV-vis. spectrum was recorded using a Perkin-Elmer Lambda 19 UV-vis. spectrometer.

--X-ray photoelectron spectra (XPS) were performed in a SPECS Sage HR 100 spectrometer with a non-monochromatic X-ray source (magnesium Kα line of 1253.6 eV energy and 252 W)

Mass Spectrometer was performed by the CESAMO on a Thermo Trace GC ultra-gas chromatograph coupled to a Thermo ISQ mass detector.

2. Synthesis of TMNP and TMNP*

Preparation of [Co(η^5-C$_5$Me$_5$) (η^4-C$_5$H$_6$)]

NaBH$_4$ (189.2 mg, 5 mmol) was added into the THF solution of Cp*CoCpPF$_6$ [1](202 mg, 0.5 mmol) in N$_2$ and subsequently, the color of the solution changed from yellow to orange to red, indicating the formation of the **2** (Equation S1). Overnight, THF was removed *in vacuo*, and 20 ml pentane was injected to dissolve **2**. Finally, **2** was purified by cannula

filtration to get the product as red solid. The yield of **2** is 90%. The formation of [Co(η^5-C$_5$Me$_5$)(η^4-C$_5$H$_6$)] is confirmed by ^{1}H NMR, ^{13}C NMR, FT-IR and ass spectrum.

$$\text{2}^+\text{PF}_6^- \xrightarrow[\text{THF}]{\text{NaBH}_4} \text{2} + \text{NaPF}_6 + \text{BH}_3 \tag{S1}$$
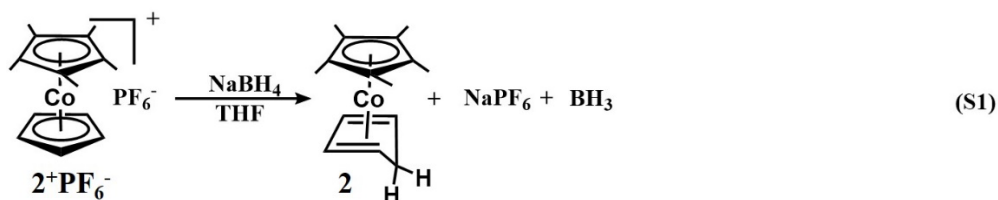
NMR: A few accurate NNR spectra of π-cyclopentadiene complexes (bonded in a tetra-hapto fashion) have been published.[2, 3] To assign the proton peaks, deuterated [Co(η^5-C$_5$Me$_5$) (η^4-C$_5$H$_5$D)] was produced by reduction of **2**$^+$**PF$_6$**$^-$ with NaBD$_4$ for comparison with **2**. As shown in Figure S1, the signal at 1.55 ppm disappears for deuterated **2^D**, indicating that the signal can be assigned to the *exo*-H (H$_4$) of the cobalt complex **2**. Subsequently, the peaks at 4.33 ppm, 2.01 ppm, 1.53 ppm and 0.83 ppm are assigned to H$_2$, H$_1$, H$_5$ and H$_3$. (Figure S1). The signal at 1.74 ppm is assigned to impurity. ^{13}C NMR in Figure **S2** shows peaks at 80.49 ppm, 49.88 ppm, 17.47 ppm, 14.13 ppm, 11.98 ppm, corresponding to -CH$_3$, -C$_5$Me$_5$ and the three C signals in cyclopentadiene.

MS: the mass spectrum shows a weak molecular peak at m/e 260.1 and the base peak at m/e 259.1. (Figure S3) The former peak corresponds to the compound **2**, while the latter peak is assigned to the hydride loss of compound **2** and the formation of stable pentamethylcobalticenium cation **2$^+$**.

FT-IR: in the FT-IR spectrum of **2**, there is a characteristic band of π-C$_5$H$_5$-metal groups, including a single C-H stretching band at 3097cm^{-1}. The bands

at 2960 cm^{-1}, 2891 cm^{-1} corresponds to the aliphatic C-H stretching frequencies. Comparing with the cationic **2$^+$PF$_6^-$**, **2** shows an unusual band at 2736 cm^{-1} and 2614 cm^{-1}, attributed to the C-H$_{endo}$ and C-H$_{exo}$ stretching frequency, owing to a steric and electrostatic interactions between Co and H$_{endo}$ / H$_{exo}$. [2] The bands at 1443~1316 cm^{-1} are recognized as the C-C stretching frequency for the cyclopentadienyl ring. (Figure S4) [5]
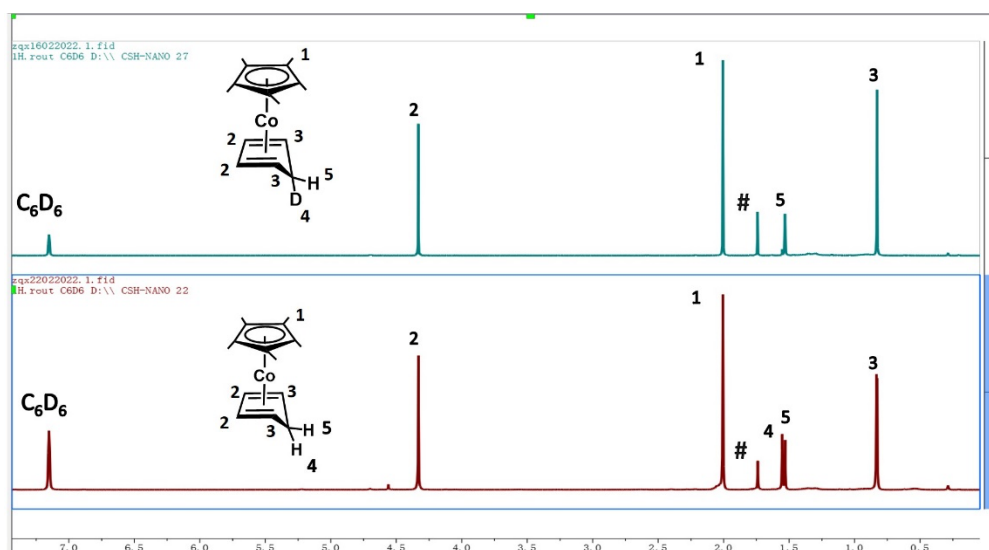

Figure S 1. ^{1}H NMR of [Co(η^5-C$_5$Me$_5$) (η^4-C$_5$H$_6$)] and [Co(η^5-C$_5$Me$_5$) (η^4-C$_5$H$_5$D)]: ^{1}H NMR (300 MHz, C$_6$D$_6$).
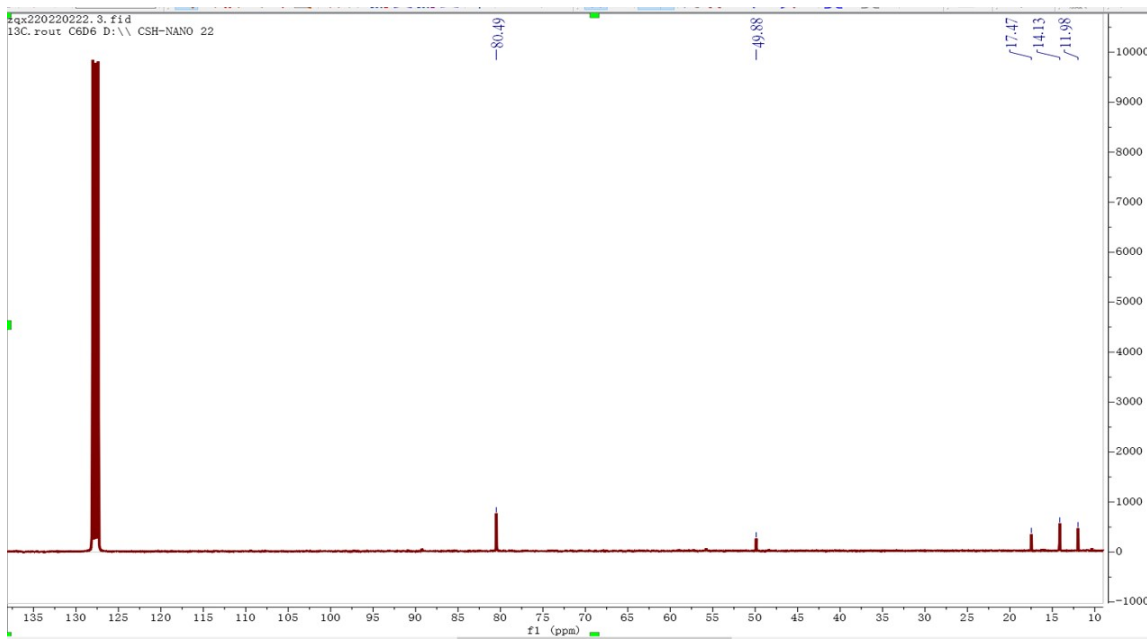
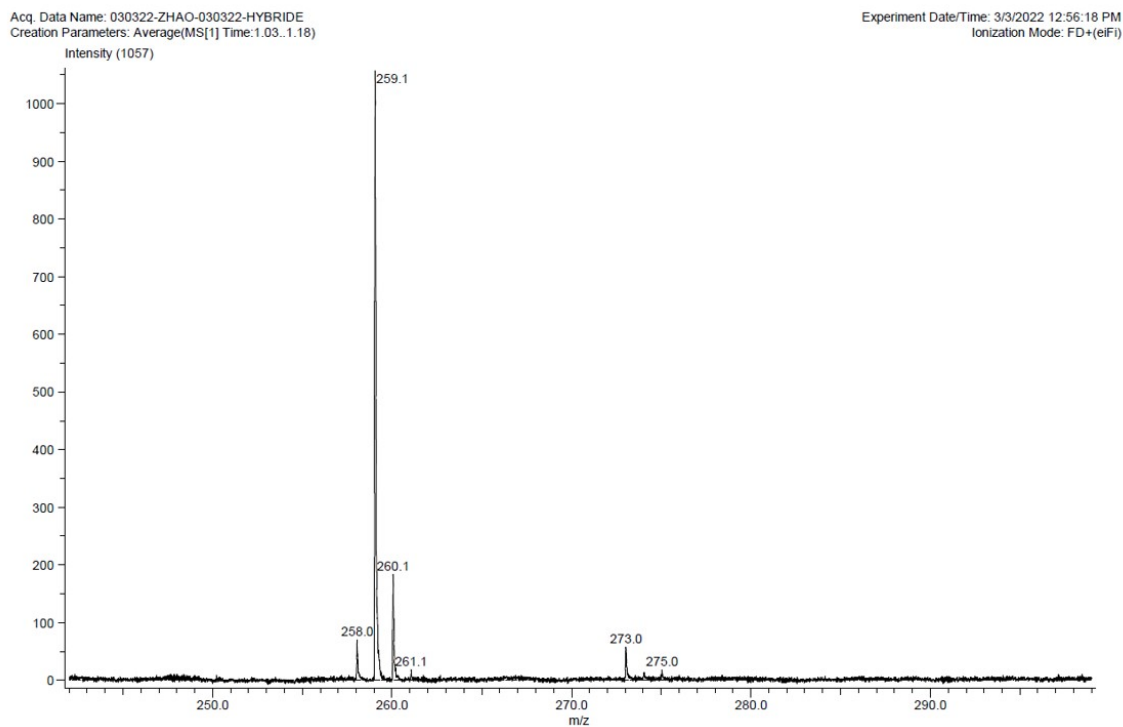**Figure S 2**. ^{13}C NMR of $[Co(\eta^5\text{-}C_5Me_5)(\eta^4\text{-}C_5H_6)]$, **2**: ^{13}C NMR (300 MHz, C_6D_6).

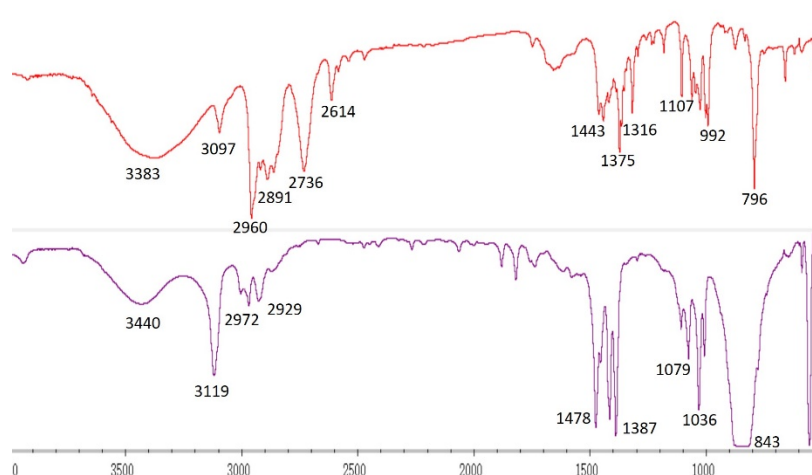**Figure S 3**. MS spectrum of $[Co(\eta^5\text{-}C_5Me_5)(\eta^4\text{-}C_5H_6)]$, **2**

**Figure S 4**. FT-IR spectrum of $[Co(\eta^5\text{-}C_5Me_5)(\eta^4\text{-}C_5H_6)]$, **2**, (upper) and $[Co(\eta^5\text{-}C_5Me_5)(\eta^5\text{-}C_5H_5)]^+PF_6^-$, **4**, (bottom)

Preparation of $[Co(\eta^5\text{-}C_5H_5)(\eta^4\text{-}C_5H_6)]$, 1

NaBH$_4$ (189.2 mg, 5 mmol) was added into the THF solution of CpCoCpPF$_6$ (167 mg, 0.5 mmol) in N$_2$ and, immediately, the color of the solution changed from yellow to red, indicating the formation of **1** (Equation **S2**).[2, 6-8] 2h later, THF was removed *in vacuo*, and 20 ml pentane was injected to dissolve **1**. Finally, **1** was purified by cannula filtration to get the compound as red solid. The yield of **1** was 90%.
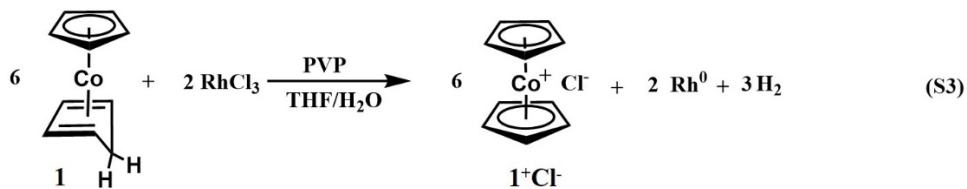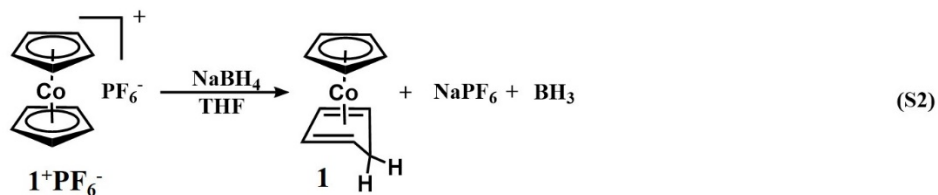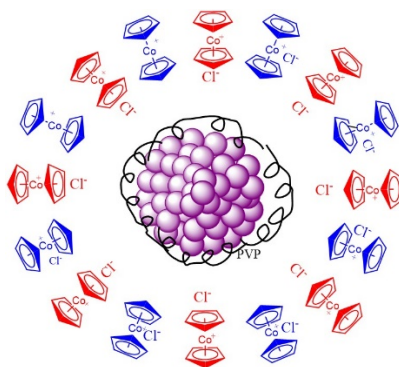
Figure S 5. Schematic illustration of RhNP upon reduction of $RhCl_3$ by $[Co(\eta^5\text{-}C_5H_5)(\eta^4\text{-}C_5H_6)]$, **1**. The red color shows coordination of Cl^- to the NP core, and the blue color shows metallocenyl chloride without coordination (corresponding to Rh atoms in the core that are not surface atoms).

3. Characterization of the TMNPs and TMNP*
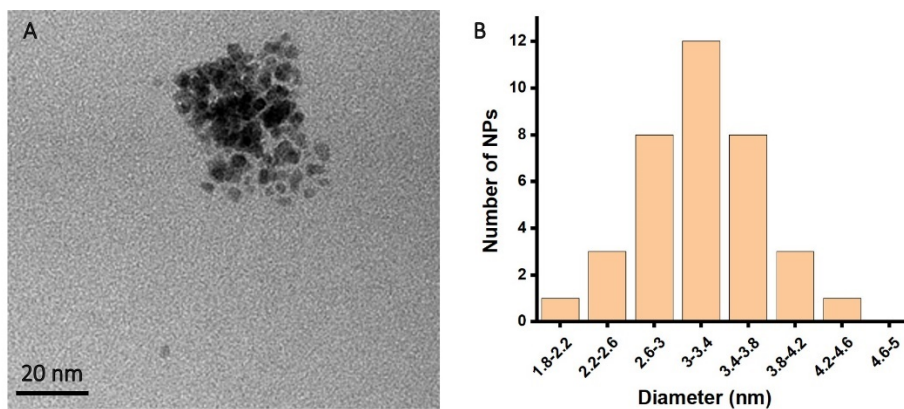
Figure S 6. TEM images and size distribution of the RhNP.
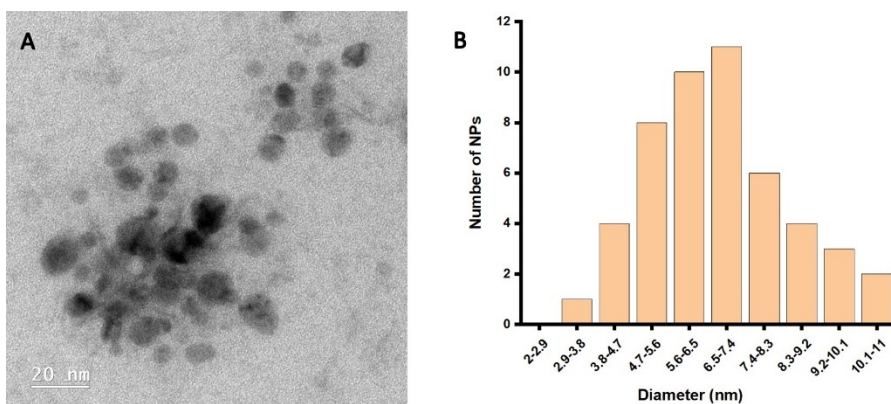
Figure S 7. TEM images and size distribution of the AuNPs*.
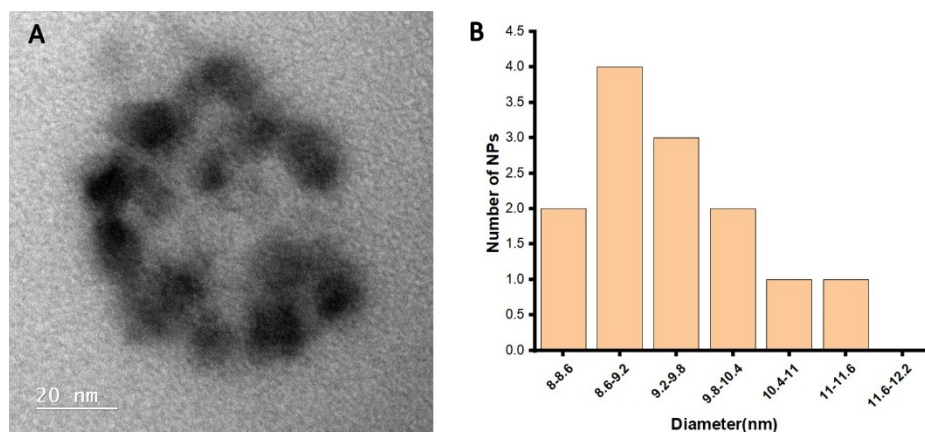
Figure S 8. TEM images and size distribution of the CuNPs*.
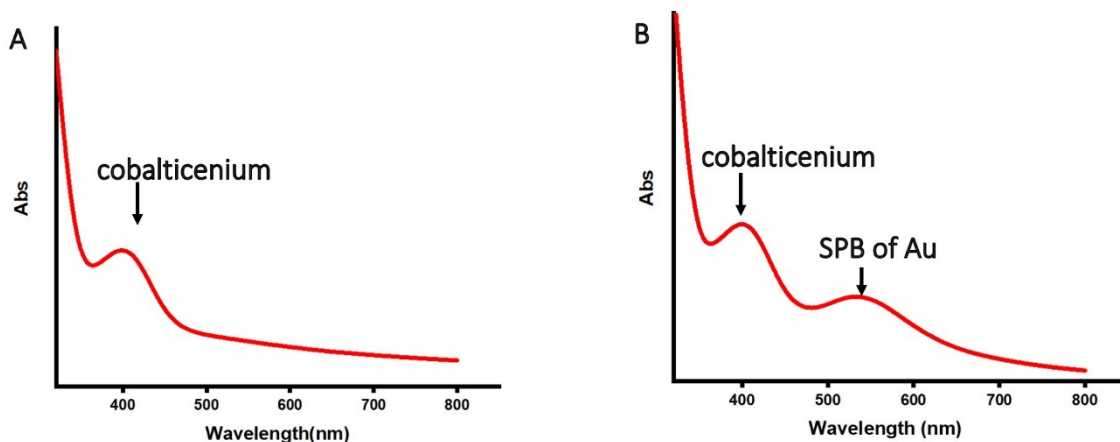
Figure S 9. UV-vis. spectra of RhNP* (A), AuNP* (B)

4. H_2 evolution from $B_2(OH)_4$ and AB hydrolysis catalysed by TMNP and TMNP*

The catalytic hydrolysis of $B_2(OH)_4$ was carried out at 20 ± 1 °C. In a typical experiment, 0.2 % mmol RhNP* (5 ml H_2O + 1 ml THF) was placed in a 50 ml round bottom flask with two outlets. Then, $B_2(OH)_4$ (1 mmol, 90 mg) dissolved in 5 ml deionized water was added under vigorous stirring. The measurement of the produced H_2 gas was conducted in a typical water-filled gas burette.

The catalytic hydrolysis of AB was carried out at 20 ± 1 °C. In a typical experiment, 0.2 % mmol RhNP* (5 ml H_2O + 1 ml THF) was placed in a 50ml round bottom flask with two outlets. Then, AB (1 mmol, 31 mg) dissolved in 1 ml deionized water was added under vigorous stirring. The measurement of the produced H_2 gas was conducted in a typical water-filled gas burette. The temperature of the reaction was measured using an electronic thermometer.

$$lnk = -\frac{Ea}{RT} + lnA \qquad (S4)$$

Calculation of the TOF per surface atom:

$$TOF_t = \frac{n_{H_2}}{n_{cat_t} \cdot time}$$

$$TOF_s = \frac{n_{H_2}}{n_{cat_s} \cdot time}$$

Where, TOF$_t$ is the turnover frequency of the total atoms. TOF$_s$ is the turnover frequency of the surface atoms. n_{H_2} is mole of produced H_2. Time is reaction time (min). n_{cat_t} is mole of total atoms. n_{cat_s} is mole of surface atoms.

When number of surface atoms N_s and the number of total atoms N_t is introduced here,

$$\frac{n_{cat_s}}{n_{cat_t}} = \frac{N_s}{N_t}$$

On the other hand,

$$N_t = \frac{\frac{4}{3}\pi R_{NP}{}^3}{\frac{4}{3}\pi R_{atom}{}^3}$$

$$N_S = \frac{4\pi R_{NP}^{2}}{\pi R_{atom}^{2}}$$

Where R_{atom} is the radius of metal atom, R_{NP} is the radius of nanoparticles.

Thus,

$$TOF_S = \frac{TOF_t \cdot R_{NP}}{4R_{atom}}$$

Table S 1. TOF values of RhNP and RhNP* in $B_2(OH)_4$ and AB hydrolysis

	$B_2(OH)_4$		AB	
	RhNP	RhNP*	RhNP	RhNP*
NP diameter(nm)	3.0	2.5	3.0	2.5
Atom diameter(nm)	0.135	0.135	0.135	0.135
TOF$_t$	579	1364	165	125
TOF$_s$	3217	6315	917	578

the unit of TOF$_t$ and TOF$_s$ is $mol_{H_2} mol_{cat}^{-1} min^{-1}$.

Table S 2. Comparison of the catalytic performances of nanocatalysts in $B_2(OH)_4$ hydrolysis

Catalyst	Support	NPs loading	TOF [a]
RhNP*	pentamethylcobalticenium	0.2mol%	6315
RhNP	cobalticenium	0.2mol%	3217
RhNP[9]	graphene quantum dots	0.4 mol‰	3658
PtNP[9]	graphene quantum dots	0.4 mol‰	4603
AuNP[9]	graphene quantum dots	0.4 mol‰	1698
PdNP[9]	graphene quantum dots	0.4 mol‰	802
IrNP[9]	graphene quantum dots	0.4mol ‰	185
RuNP[9]	graphene quantum dots	0.4 mol‰	127
Glucan-PtNP[9]	Glucan	0.4 mol‰	830
TiO_2-PtNP[9]	TiO_2	3.66 wt %	681
Pt/C[9]	Carbon	5.0 wt %	300
Rh@dendrimer[10]	dendrimer	0.1mol%	132

[a] TOF = TOF_s= $mol_{H_2\ produced}$ / [surface mol_{cat_t}× reaction time (min)] the unit is $mol_{H_2}\ mol_{cat}^{-1}\ min^{-1}$.

Table S 3. Comparison of catalytic performance of RhNPs anchored on different supports in AB hydrolysis

Catalyst	Support	NPs loading	TOF [a]
RhNP*	pentamethylcobalticenium	0.2%	578
RhNP	cobalticenium	0.2%	917
RhNPs/dendrimer[11]	Dendrimer	1%	244
RhNPs/THPP[12]	THPP	0.2%	132
GQDs -RhNPs[13]	GQDs	0.4%	642
Rh_1/VO_2 [14]	VO_2 nanorods	0.2%	48
Rh^0/CeO_2[15]	CeO_2	0.8%	2010
Rh^0/SiO_2[15]	SiO_2	0.8%	112
Rh^0/Al_2O_3[15]	Al_2O_3	0.8%	195
Rh^0/TiO_2[15]	TiO_2	0.8%	105
Rh^0/ZrO_2[15]	ZrO_2	0.8%	102
Rh^0/HfO_2[15]	HfO_2	0.8%	24
Rh(0)/CNT[16]	CNT	0.25%	706
Rh/graphene[17]	Graphene	0.4%	325
$Rh(0)@TiO_2$[18]	TiO_2	0.116%	260

[a] TOF = $mol_{H_2\ produced}$ / [surface mol_{cat_t}× reaction time (min)], the unit is $mol_{H_2}\ mol_{cat}^{-1}\ min^{-1}$.

5. Mechanistic studies of AB hydrolysis catalysed by RhNP*

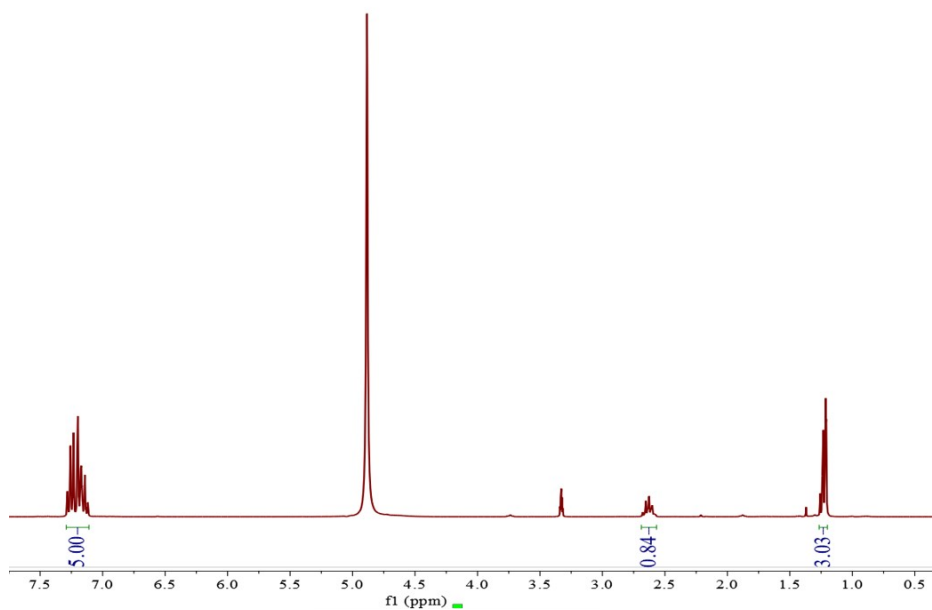**Figure S 10**. ^{1}H NMR spectrum of the hydrogenation product of styrene in CD$_3$OD. 1H NMR (300 MHz, CD$_3$OD) δ 7.12~7.28 ppm (CH-arom, 5.00H), 2.67~2.58ppm (-CH2, 0.84H), 1.21~1.25 ppm (-CH3, 3.03H).

6. References

S1. V. Martinez, J.-C. Blais, G. Bravic and D. Astruc, Coupling Multiple Benzylic Activation of Simple Arenes by CpFe[+] with Multiple Alkene Metathesis Using Grubbs Catalysts: An Efficient Carbon–Carbon Bond Formation Strategy Leading to Polycycles, Cyclophanes, Capsules, and Polymeric Compounds and Their CpFe[+] Complexes, *Organometallics*, 2004, **23**, 861-874.

S2. M. L. H. Green, L. Pratt and G. Wilkinson, 760. A new type of transition metal–cyclopentadiene compound, *Journal of the Chemical Society (Resumed)*, 1959, DOI: 10.1039/JR9590003753, 3753-3767.

S3. R. K. Kochhar and R. Pettit, Cyclopentadieneiron tricarbonyl, *J. Organomet. Chem.*, 1966, **6**, 272-278.

S4. K. Moseley, J. W. Kang and P. M. Maitlis, Pentamethylcyclopentadienyl-rhodium and -iridium halides. Part II. Reactions with mono-, di-, and tri-olefins, *J. Chem. Soc. A*, 1970, DOI: 10.1039/J19700002875, 2875-2883.

S5. T. S. Piper and G. Wilkinson, Alkyl and aryl derivatives of π-cyclopentadienyl compounds of chromium, molybdenum, tungsten, and iron, *J. Inorg. Nucl. Chem.*, 1956, **3**, 104-124.

S6. F. Fu, Q. Wang, R. Ciganda, A. M. Martinez-Villacorta, A. Escobar, S. Moya, E. Fouquet, J. Ruiz and D. Astruc, Electron- and Hydride-Reservoir Organometallics as Precursors of Catalytically Efficient Transition Metal Nanoparticles in Water, *Chem. Eur. J*, 2018, **24**, 6645-6653.

S7. F. Fu, A. Dedieu, W. Wang, T. Chen, Y. Song, E. Fouquet, J. R. Hamon, M. Zhu and D. Astruc, Stabilization of a new nanocomposite family by reduction of gold nanoclusters with electron-reservoir complexes, *Chem. Commun.*, 2019, **55**, 10277-10280.

S8. L. P. Szajek and J. R. Shapley, Unexpected synthesis of CpIr(.eta.4-C5H6) and a proton and carbon-13 NMR comparison with its cobalt and rhodium congeners, *Organometallics*, 1991, **10**, 2512-2515.

S9. W. Chen, J. Shen, Y. Huang, X. Liu and D. Astruc, Catalyzed Hydrolysis of Tetrahydroxydiboron by Graphene Quantum Dot-Stabilized Transition-Metal Nanoparticles for Hydrogen Evolution, *ACS Sustain. Chem. Eng.*, 2020, **8**, 7513-7522.

S10.   Q. Zhao, N. Kang, M. Martínez Moro, E. Guisasola, S. Moya, E. Coy, L. Salmon, X. Liu and D. Astruc, Sharp Volcano-Type Synergy and Visible Light Acceleration in H_2 Release upon $B_2(OH)_4$ Hydrolysis Catalyzed by Au-Rh@Click-Dendrimer Nanozymes, *ACS A.E.M*, 2022, **5**, 3834–3844.

S11.   Q. Wang, F. Fu, A. Escobar, S. Moya, J. Ruiz and D. Astruc, "Click" Dendrimer-Stabilized Nanocatalysts for Efficient Hydrogen Release upon Ammonia-Borane Hydrolysis, *ChemCatChem*, 2018, **10**, 2673-2680.

S12.   N. Zhang, G. Liu, Y. Sun, Y. Wang, J. Yan and X. Liu, H_2 Evolution Upon Hydrolysis of Ammonia-Borane Catalyzed by Porphyrin Stabilized Nanocatalysts, *Catal. Lett.*, 2021, **151**, 2272-2278.

S13.   J. Shen, W. Chen, G. Lv, Z. Yang, J. Yan, X. Liu and Z. Dai, Hydrolysis of NH_3BH_3 and $NaBH_4$ by graphene quantum dots-transition metal nanoparticles for highly effective hydrogen evolution, *Int. J. Hydrog. Energy*, 2021, **46**, 796-805.

14.L. Wang, H. Li, W. Zhang, X. Zhao, J. Qiu, A. Li, X. Zheng, Z. Hu, R. Si and J. Zeng, Supported Rhodium Catalysts for Ammonia–Borane Hydrolysis: Dependence of the Catalytic Activity on the Highest Occupied State of the Single Rhodium Atoms, *Angew. Chem. Int. Ed.*, 2017, **56**, 4712-4718.

S15.   S. Akbayrak, Y. Tonbul and S. Özkar, Ceria supported rhodium nanoparticles: Superb catalytic activity in hydrogen generation from the hydrolysis of ammonia borane, *Appl. Catal. B*, 2016, **198**, 162-170.

S16.   D. W. Himmelberger, C. W. Yoon, M. E. Bluhm, P. J. Carroll and L. G. Sneddon, Base-Promoted Ammonia Borane Hydrogen-Release, *J. Am. Chem. Soc.*, 2009, **131**, 14101-14110.

S17.   J. Shen, L. Yang, K. Hu, W. Luo and G. Cheng, Rh nanoparticles supported on graphene as efficient catalyst for hydrolytic dehydrogenation of amine boranes for chemical hydrogen storage, *Int. J. Hydrog. Energy*, 2015, **40**, 1062-1070.

S18.   S. Akbayrak, S. Gençtürk, İ. Morkan and S. Özkar, Rhodium(0) nanoparticles supported on nanotitania as highly active catalyst in hydrogen generation from the hydrolysis of ammonia borane, *RSC Adv.*, 2014, **4**, 13742-13748.